



Single Particle Imaging. Simulation.

Alexey Khudorozhkov

Moscow Institute of Physics and Technology, Dolgoprudniy, Russia

Supervisors: Max Rose, Dmitry Dzhigaev, Ivan Vartanians

DESY, Hamburg, Germany

Wednesday 7th September, 2016

Abstract

For different purposes of structural biology and material science a proper way for investigation of the structure of nano-size objects (e.g. viruses) is needed. One of the common methods for revealing structure of biological specimens is X-ray crystallography. However, it has some disadvantages. The most important one is that not all biological specimens could be crystallized. That is why single particle imaging (SPI) becomes high-demand. One can irradiate a single object with X-ray pulse obtaining all needed information from collected diffraction patterns. Although SPI is a very promising technique, it is not up-to-the-mark developed yet for achieving significant results. In the present work we simulate the experiment on single particle imaging of the Rice Dwarf Virus (RDV) in order to determine the input parameters for obtaining sensible results about the structure of the virus. Additionally, we estimate the resolution limits of the final structure depending on input parameters.

Contents

1.	Introduction	3
2.	SPI experiment stages	4
2.1.	Real experiment	4
2.2.	Experiment simulation	4
3.	Theory and simulation design	5
3.1.	Scattering theory	5
3.2.	Geometry of the experiment	8
3.3.	Procedure of stacking	8
3.4.	Simulation parameters	11
3.5.	Resolution	11
3.6.	The quality of reconstruction	12
4.	Simulation Results	12
5.	Conclusion	16
6.	Acknowledgements	16
Appendix A. Fourier transform		18

1. Introduction

One of the reasons why X-ray crystallography is widely used for revealing structure of nano-size biological objects, such as viruses or biomolecules, is the lack of scattered signal from the single object. A crystal lattice is made of similar bio-objects and irradiated with X-rays giving diffraction patterns. A lot of information could be obtained from those diffraction patterns because the intensity of Bragg peaks grows quadratically due to the linear increase in the number of objects in the lattice. However, X-ray crystallography has some disadvantages, such as:

- Not all biological specimens could be arranged in a crystal lattice.
- Usually it is possible to orient in the same way only the outer shell (capsid) of viruses but not the inner proteins which account for the DNA. So, only the structure of the outer shell could be investigated.
- Usually biological samples have to be cooled down or modified somehow in order to be arranged in a crystal lattice. It means that one can not examine the virus in its natural conditions.

These are the reasons why a new technology called *single particle imaging* (SPI) looks promising. A single object is irradiated with X-rays. Although this irradiation destroys the sample, nowadays, due to the development of free electron lasers (see, for example, [1] or [2]), it is possible to create a pulse short and powerful enough to obtain needed information before the destruction. This method is called "Diffract-and-Destroy". It was theoretically described in 2000 [3] and its usefulness was experimentally proved in 2006 [4].

However, the resolution obtained using SPI can not yet compete with the resolution obtained with crystallography methods. That is the reason why we want to simulate an experiment and estimate the correspondence between input parameters and the resolution of the final image.

2. SPI experiment stages

Here we will briefly describe the stages of a real experiment on a virus and compare them to the stages of our simulation.

2.1. Real experiment

The experiment is conducted on a free electron laser. For the further reconstruction many diffraction patterns corresponding to different random orientations of the sample are needed. As far as the sample is destroyed after the irradiation a lot of similar single samples should be prepared. They are injected as a flow into the space where they meet coherent X-ray beam. Scattered radiation is measured by a far-field detector and the diffraction patterns are collected from it.

Naturally there might be some corrupted patterns which correspond to situations when two or more viruses were stuck together or when the virus was too far from the centre of the beam. So, the sorting procedure is required. It could be done manually or it could be only started manually and continued automatically by the implementation of machine learning. After we have sorted out 'good' patterns we need to estimate the orientation for each of them because the viruses were oriented randomly. One of the most reliable algorithms for orientation determination is EMC [5] which stands for 'Expansion-Maximization-Compression'. After applying EMC we have many diffraction patterns with known orientation for each of them. We stack these diffraction patterns into 3D reciprocal space in order to get 3D Fourier transform of the real object's electron density. But before applying the inverse Fourier transform we need to determine the phase of each point (the information about the phase was not captured by the detector). For this purpose the so-called *phase problem* should be solved. It can be solved using phase retrieval iterative algorithms. And finally after applying inverse Fourier transform we would get the electron density 3D image in real space.

See Figure 1.

2.2. Experiment simulation

In the simulation we obtain the atomic structure of the Rice Dwarf Virus from the Protein Data Bank (PDB) [6]. After that we simulate the X-ray scattering on this structure using program MOLTRANS provided by Edgar Weckert. However, diffraction patterns are already obtained with known orientations. For this reason we do not use EMC algorithm in our simulation. We also skip the 'sorting' stage assuming that all of our diffraction patterns are 'good'. As a final stage we reconstruct the electron density of the virus solving the phase problem and applying inverse Fourier transform (reconstruction code was provided by Dmitry Dzhigaev).

For the comparison see Figure 2.

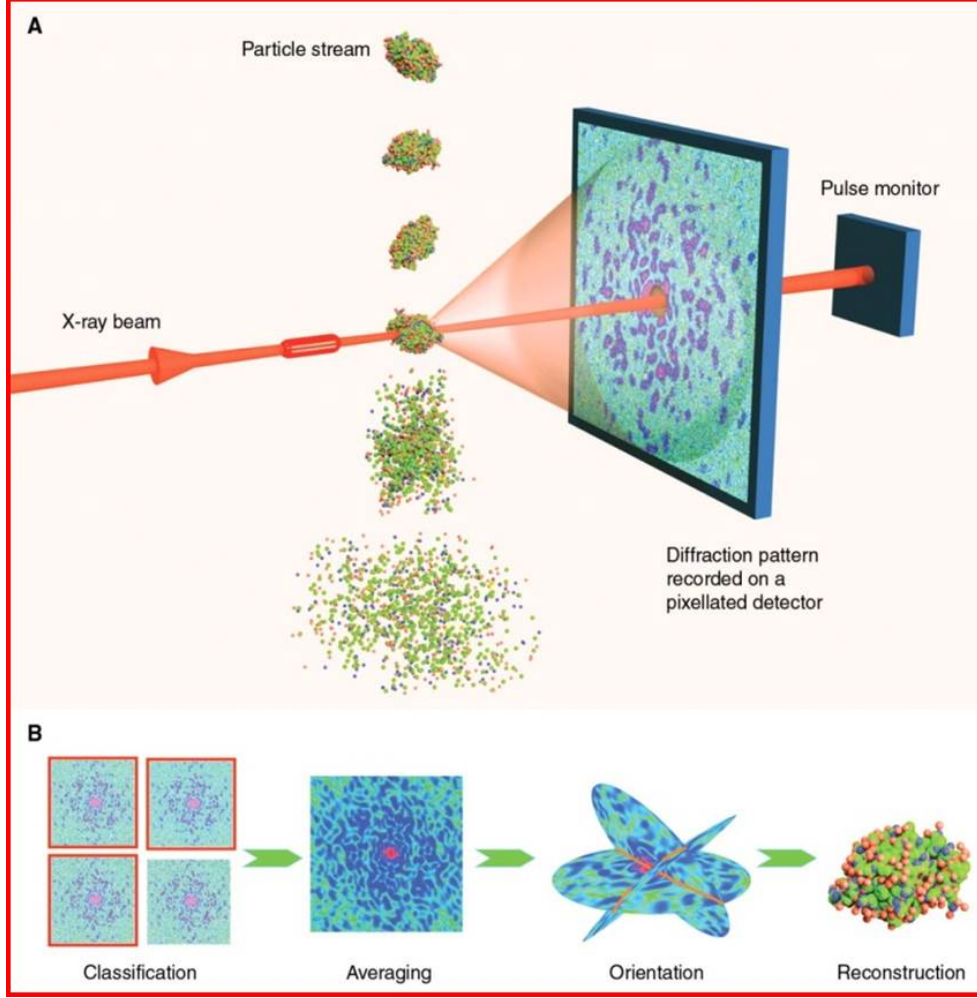


Figure 1: Experimental design adopted from [4]. (A) Experimental set-up. (B) Experiment stages.

3. Theory and simulation design

3.1. Scattering theory

First of all, we assume that only elastic scattering takes place. Let us consider the virus is an object with continuous electron density $\rho(\vec{r})$ (we will speak about it in terms of infinitesimal volume cells with charges). Interatomic distances in the virus are assumed to be small compared to the distance to the observation point. Thus, the radiation scattered from the virus is considered to be the superposition of those scattered from each volume cell with the same magnitude contribution. However, interatomic distances are comparable to the wavelength which means that phase shifts of different outgoing waves are determined by the distribution of electron density in space. This gives rise to the diffraction pattern.

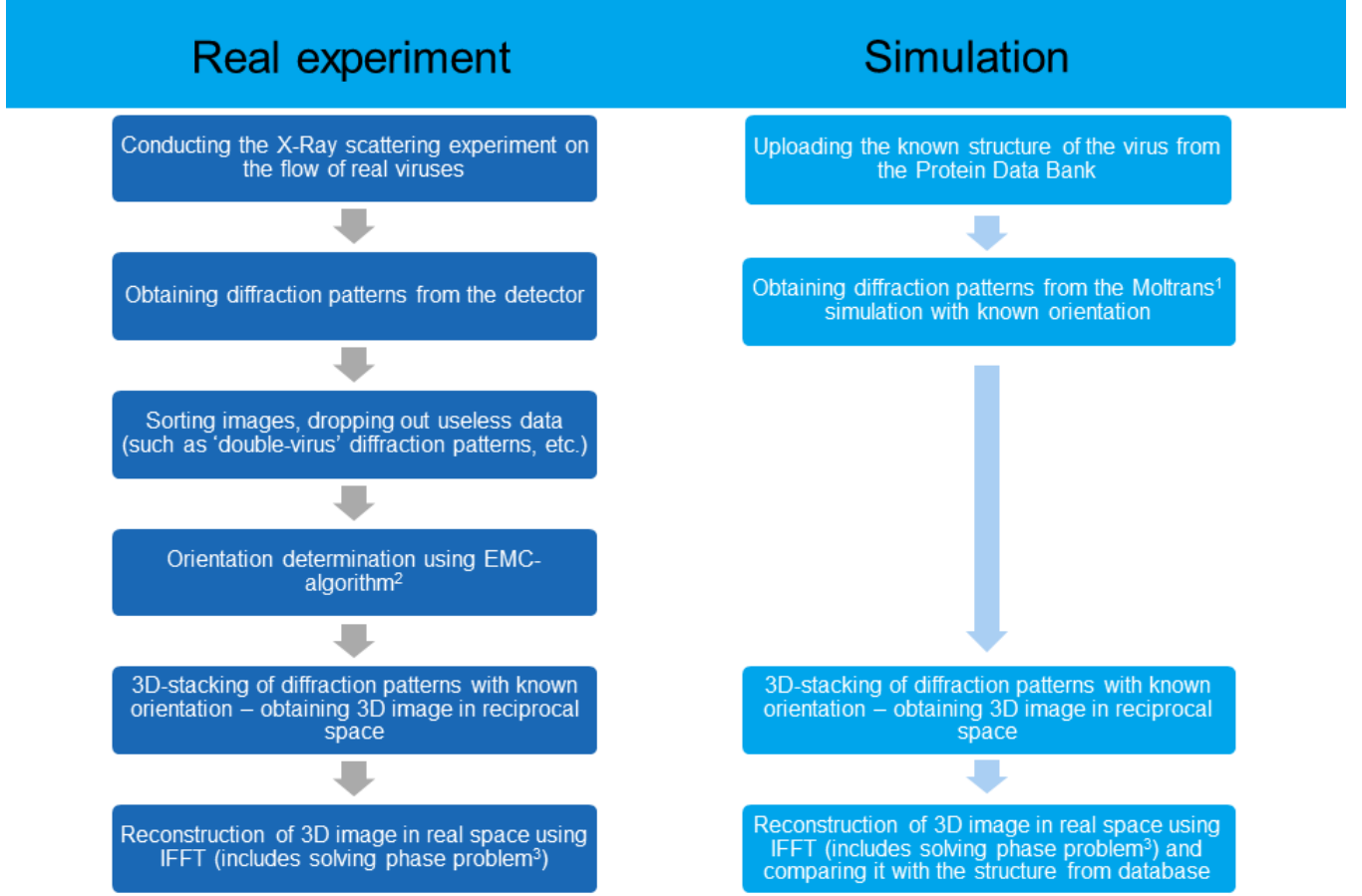


Figure 2: Flowchart with the stages of SPI experiment and its simulation

The incoming radiation is assumed to be a plane wave. Each volume cell scatters this radiation and the outgoing radiation could be decomposed into a set of plane waves (usually with continuous angular distribution). That is true for every volume cell, therefore the outgoing plane wave of a particular spatial frequency is contributed by the plane waves of the same spatial frequency from all volume cells (which propagate from the same point of space but contribute different phase shifts as stated in the previous paragraph).

Let us look at the scattering process from two volume cells (assuming one of them being placed around the origin) in the same direction (see Figure 3). The phase difference between these two waves after the scattering is

$$\Delta\varphi(\vec{r}) = \vec{k}_{in} \cdot \vec{r} - \vec{k}_{out} \cdot \vec{r} = -\vec{q} \cdot \vec{r}, \quad (1)$$

where vector $\vec{q} = \vec{k}_{out} - \vec{k}_{in}$ is called wavevector transfer. The resulting scattered ampli-

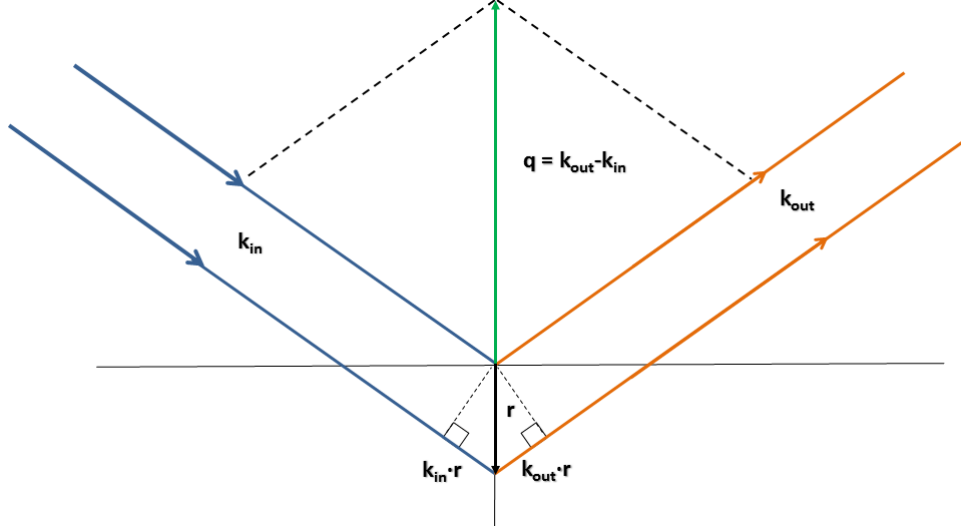


Figure 3: Scattering from two volume cells in the same direction. \vec{k}_{in} - wavevector of the incident wave, \vec{k}_{out} - wavevector of the scattered wave, \vec{q} - wavevector transfer

tude from the sample is proportional to

$$A(\vec{q}) = \int_V \rho(\vec{r}) e^{-i\vec{q} \cdot \vec{r}} d\vec{r}^3 \quad (2)$$

(if our sample was an atom, $A(\vec{q})$ would be known as the atomic form factor). One may notice that the equation (2) is the Fourier transform of the electron density (for Fourier transform see Appendix A).

When the next condition is valid:

$$\frac{d^2}{\lambda z} \ll 1, \quad (3)$$

where z is the distance from the virus to the observation point, λ is the wavelength and d is the representative size of the object, the Fraunhofer diffraction takes place [13]. It means that each plane wave in the object plane corresponds to the point in the detector plane. Thus, the amplitude in a particular point of the detector is unequivocally connected with \vec{k}_{out} and therefore with \vec{q} and could be calculated using (2).

However, the detector measures not the amplitude but the intensity which is

$$I(\vec{q}) = |A|^2(\vec{q}). \quad (4)$$

Note that the phase of the wavefield is lost. This problem is called *the phase problem* and could be solved using iterative phase retrieval algorithms.

The main conclusion from the theory is that we have the unequivocal correspondence between the electron density in real space and vectors \vec{q} in the new space which is

called *the reciprocal space*. Since we can obtain the information about the reciprocal space from the detector (and solve the phase problem) we could reconstruct the initial electron density of the sample.

3.2. Geometry of the experiment

For the experiment geometry description we treat the virus as a point because we assume that Fraunhofer diffraction takes place. On the sphere S (every point on it has the same optical path length from the virus) equidistant steps correspond to equidistant angular steps and therefore to equidistant \vec{q} -steps in the reciprocal space. If we imagine that we had a detector with the shape of a sphere we would stack the pictures from this detector as planes in reciprocal space. But in a real experiment (as well as in our simulation) the detector is plane, equidistant steps in the detector plane do not correspond to equidistant steps in reciprocal space. Thus, during the stacking we need to curve the plane picture from the detector into spherical sector as shown in Figure 4. The coordinate transformation is the following

$$x' = \frac{Lx}{\sqrt{L^2 + x^2 + y^2}} \quad (5)$$

$$y' = \frac{Ly}{\sqrt{L^2 + x^2 + y^2}} \quad (6)$$

$$z' = L - \frac{L^2}{\sqrt{L^2 + x^2 + y^2}}, \quad (7)$$

where L is the distance from the virus to the detector.

3.3. Procedure of stacking

For every diffraction pattern created by MOLTRANS we know 3 Euler angles which determine how the virus was rotated.

The Euler angles determine the orientation of the object in the following way (see Figure 5): let us assume that x, y, z are the coordinate axes before rotation and X, Y, Z are the coordinate axes after rotation, also the line of nodes N is defined as the intersection of xy and XY coordinate planes. Then Euler angles are defined in the following way:

- α (or φ) is the angle between the x axis and the N axis (the angle of precession).
- β (or θ) is the angle between the z axis and the Z axis (the angle of nutation).
- γ (or ψ) is the angle between the N axis and the X axis (the angle of intrinsic rotation).

One of the possibilities to reach the final state of rotated object using Euler angles is to rotate it the following way:

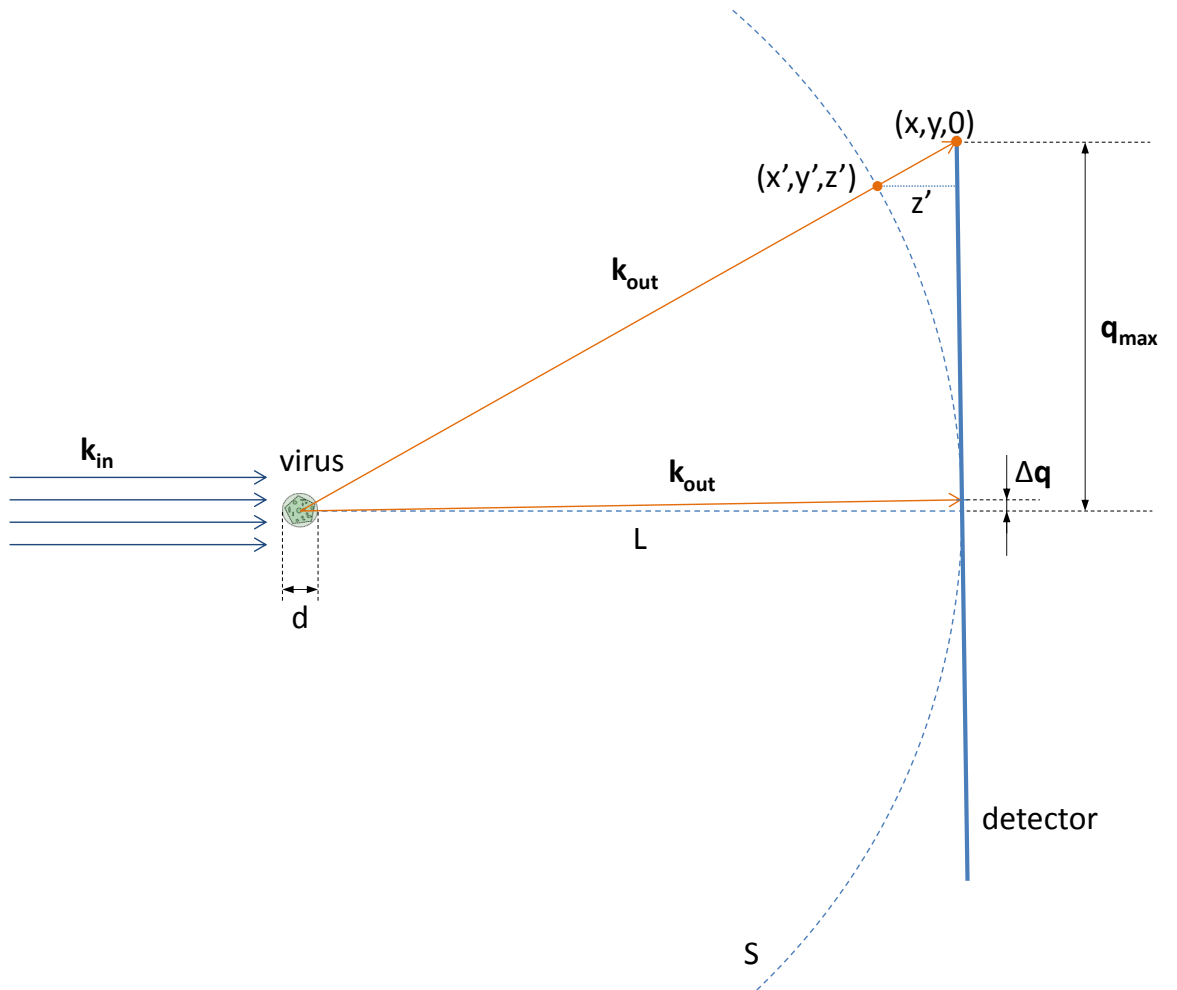


Figure 4: Geometry of the experiment. The picture from the detector should be curved into spherical sector. A point with coordinates $(x, y, 0)$ turns into a point with coordinates (x', y', z') .

1. Around axis z by angle γ
2. Around axis x by angle β
3. Around axis z by angle α

(where z and x are fixed axes as shown in the Figure 5 and all rotations are done clockwise).

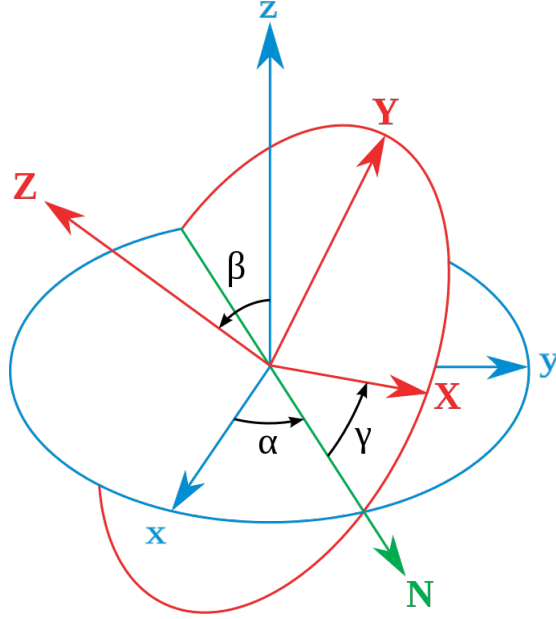


Figure 5: The definition of Euler angles [8].

So, the new coordinates could be calculated using matrix of rotation M [9]:

$$M = \begin{pmatrix} \cos \alpha \cos \gamma - \sin \alpha \cos \beta \sin \gamma & -\cos \alpha \sin \gamma - \sin \alpha \cos \beta \cos \gamma & \sin \alpha \sin \beta \\ \sin \alpha \cos \gamma + \cos \alpha \cos \beta \sin \gamma & -\sin \alpha \sin \gamma + \cos \alpha \cos \beta \cos \gamma & -\cos \alpha \sin \beta \\ \sin \beta \sin \gamma & \sin \beta \cos \gamma & \cos \beta \end{pmatrix} \quad (8)$$

$$\begin{pmatrix} x' \\ y' \\ z' \end{pmatrix} = M \cdot \begin{pmatrix} x \\ y \\ z \end{pmatrix} \quad (9)$$

If the virus was rotated around axes $z-x-z$ by angles γ, β, α correspondingly, we would rotate the diffraction pattern around axes $z-x-z$ by angles $-\alpha, -\beta, -\gamma$ correspondingly (the opposite sequence of rotations and the opposite direction of angles). That means that one needs to replace angles in the matrix of rotation M the next way: $\alpha \rightarrow (-\gamma), \beta \rightarrow (-\beta), \gamma \rightarrow (-\alpha)$.

The stacking procedure is performed the following way: the value from each pixel on a diffraction pattern is assumed to be in the centre of its pixel, then coordinates are transformed as shown in 5, 6, 7, after that the rotation 9 (with proper angles) is applied. Then values of the points which lie inside the same voxel are averaged. There may be some 'empty' voxels which do not contain any value. Of course one could interpolate all points with values onto a 3D grid but this process takes much more time and memory. That is why we just assume that 'empty' voxels correspond to zero values.

When 3D reciprocal space is stacked, phase retrieval algorithms could be applied in order to reconstruct electron density distribution in real space. In the present paper we

do not discuss how phase retrieval algorithms work. For such information see [10]. In our work we used the program PHASOR (Error Reduction algorithm and Hybrid Input Output algorithm) kindly provided by Dmitry Dzhigaev.

3.4. Simulation parameters

In our simulation we used the following set of parameters:

- Distance from the virus to the detector (z): 323 mm.
- The side length of the square plane detector (D): 258 mm.
- The wavelength (λ): 7.75 Å.
- The number of pixels on the detector ($N \times N$): 220×220 pixels.
- Fluence: 10^{13} , 10^{10} photons per μm^2 per pulse; and also evenly distributed random fluence for each diffraction pattern within the boundaries $10^9 - 10^{10}$ photons per μm^2 per pulse.
- Poisson noise can be added to each diffraction pattern.
- Number of diffraction patterns: 1000, 5000, 10 000, 40 000.
- Beam focus: 2 μm in diameter.

For every number of diffraction patterns given above all fluence values (also given above) were applied. The random distribution of fluence was implemented to mimic the fact that the beam intensity is not constant but varying over time and space.

3.5. Resolution

Kotelnikov-Shannon-Whittaker sampling theorem states that a band-limited signal (Fourier transform of this signal is zero outside the finite region of frequencies) can be perfectly reconstructed from an infinite sequence of samples if the sampling rate exceeds two samples per period of the highest frequency in the initial signal [12]. From this theorem we could say that if you want to recover a feature of the size Δl in an image, you need to sample the corresponding interference fringes in reciprocal space with at least two pixels per fringe. So, the resolution in reciprocal space must not be less than $\Delta q = \pi/\Delta l$. The achievable resolution in real space is theoretically limited by the highest measured spatial frequency and can be calculated as

$$\Delta x = \frac{\lambda z}{D}. \quad (10)$$

Thus, the highest spatial frequency is

$$q_{max} = \frac{1}{2\Delta x}. \quad (11)$$

Then the step of the grid in reciprocal space is the following

$$\Delta q = \frac{q_{max}}{(N/2)}. \quad (12)$$

In our case $\Delta x \approx 0.97$ nm. However, in a real experiment the resolution depends on the biggest scattering angle where a significant signal could be measured. So, for estimation of the resolution limits the Power Spectral Density (PSD) function was used. This function averages the signal from voxels of the same distance from the centre in reciprocal space.

3.6. The quality of reconstruction

Because of the fact that the phase retrieval algorithm depends a lot on some intrinsic parameters and the number of iterations used, one could not easily reconstruct the object with the best possible quality - for that some experience in tuning the parameters is needed. After the reconstruction Phase-Retrieval Transfer Function (PRTF) was used to estimate the quality of the reconstruction. This function takes the Fourier transform of reconstructed object ($O(\vec{r})$) and compares it to the values in initial reciprocal space ($\sqrt{I(\vec{q})}$) in the following way:

$$PRTF(\vec{q}) = \frac{|FT[O(\vec{r})]|}{\sqrt{I(\vec{q})}}, \quad (13)$$

where $FT[\dots]$ denotes Fourier transform (see Appendix A). When this function equals 1 that means that the best possible quality of reconstruction for a given \vec{q} value is reached.

4. Simulation Results

Let us show the results of each simulation stage through the example with fluence 10^{13} photons per μm^2 per pulse (with noise). A typical diffraction pattern obtained with MOLTRANS is shown in Figure 6(a) and after stacking diffraction patterns in 3D reciprocal space the middle cut of this space is shown in Figure 6(b). The isosurface of the reciprocal space is represented in Figure 7.

The PSD plots calculated from the reciprocal space are shown in Figure 8. It is an ambiguous questions how to estimate the resolution limit from the PSD plot. Since the standard deviation of Poisson noise is equal to the square root of the average number of events N , the signal-to-noise ratio (SNR) is given by

$$SNR = \frac{N}{\sqrt{N}} = \sqrt{N}. \quad (14)$$

One of the possibilities is to set the limit at the point where the PSD reaches SNR of a particular value. In our simulation we used $SNR = 5$.

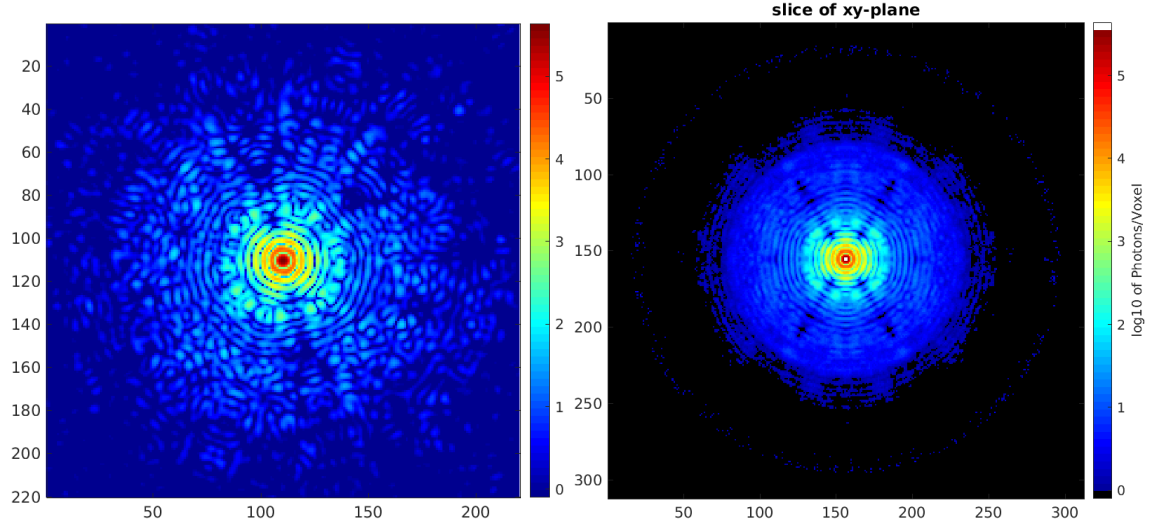


Figure 6: (a) Diffraction pattern. Fluence - 10^{13} photons per μm^2 per pulse, with noise. (b) Cut through the centre of stacked reciprocal space. 40 000 diffraction patterns, fluence - 10^{13} photons per μm^2 per pulse, with noise.

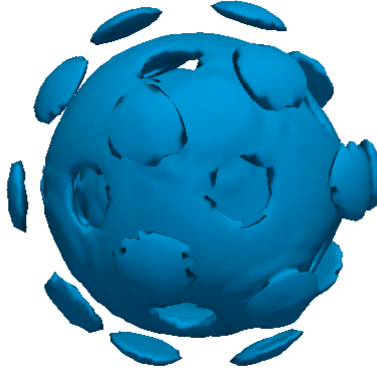


Figure 7: One of the isosurfaces in 3D reciprocal space. 40 000 diffraction patterns, fluence - 10^{13} photons per μm^2 per pulse, with noise.

At the next stage the reconstruction algorithm took place and the result (isosurface of the electron density) is shown in the Figure 9(a). And we can compare it with the image taken from Protein Data Bank (Figure 9(b)). We could estimate the quality of the reconstruction by looking at PRTF (Figure 10). One could see that the reconstruction is quite far from ideal, though the main symmetry of the virus is seen.

Hereafter, we will compare resolution limits for all datasets created. See Table 1. As one can see, the resolution limit is getting better with increasing the fluence or increasing

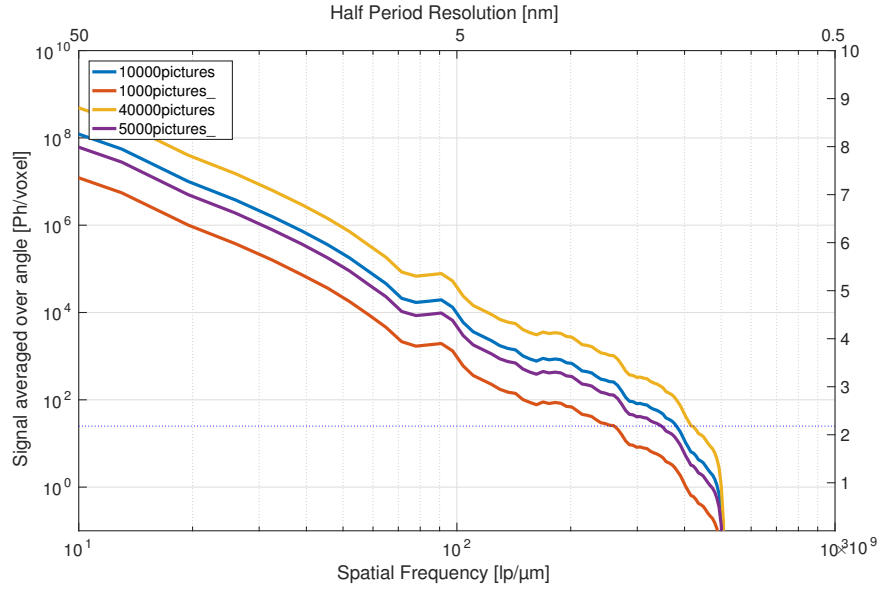


Figure 8: PSD plots for different numbers of diffraction patterns. Fluence - 10^{13} photons per μm^2 per pulse, with noise.

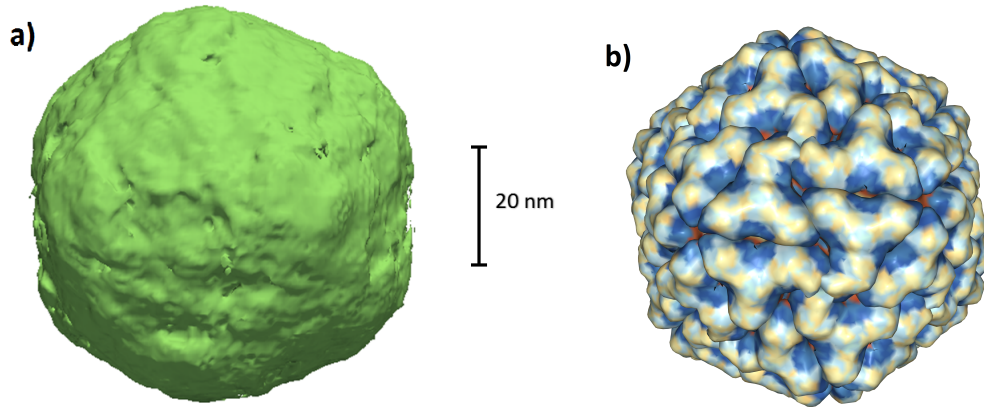


Figure 9: (a) One of the isosurfaces in real space after reconstruction. 40 000 diffraction patterns, fluence - 10^{13} photons per μm^2 per pulse, with noise. (b) The image of the virus taken from Protein Data Bank [6].

the number of diffraction patterns.

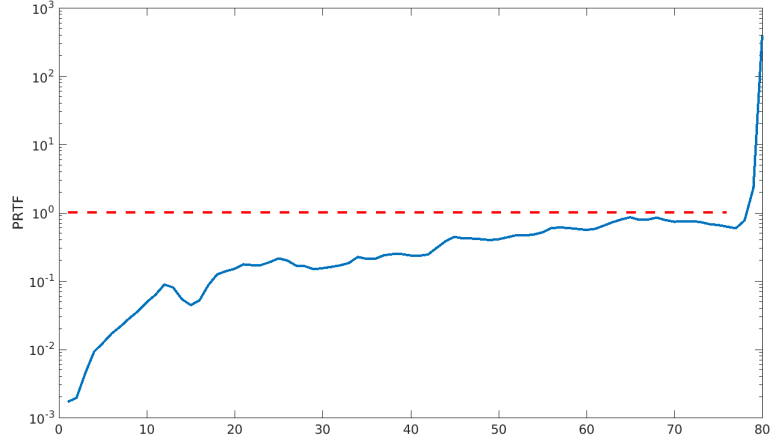


Figure 10: Phase-Retrieval Transfer Function. The closer the function to 1 - better the quality of reconstructed object. 40 000 diffraction patterns, fluence - 10^{13} photons per μm^2 per pulse, with noise.

Table 1: Resolution limits in nm. On the left - the number of diffraction patterns. On the top - the fluence in photons per μm^2 per pulse. All datasets - with noise.

	10^{13}	10^{10}	$10^9 - 10^{10}$
1000	1.9	9.6	11.0
5000	1.4	7.7	8.6
10 000	1.3	7.0	7.0
40 000	1.2	4.8	4.8

5. Conclusion

Recent work contains simulation of the experiment on single particle imaging of Rice Dwarf Virus (the model was taken from Protein Data Bank [6]). 1000, 5000, 10 000 and 40 000 diffraction patterns datasets for different fluence of the beam were created using MOLTRANS. Also Poisson noise was applied. The diffraction patterns were stacked into 3D reciprocal space. After that the resolution limit of reconstructed virus for each dataset was calculated using Power Spectral Density plot (see Table 1). The electron density of the virus was reconstructed using phase retrieval algorithms. Although the reconstruction quality depends a lot on intrinsic parameters of phase retrieval algorithms and the number of iterations which should be selected a posteriori, PRTF could be used to estimate the quality of the reconstruction.

Further steps of this work could contain the implementation of a beamstop and 'broken' pixels, increasing the number of diffraction patterns, the detector size and number of pixels in the detector and estimation of the highest resolution which could be obtained in SPI experiments using modern free electron lasers (such as near-built European X-Ray Free Electron Laser [1]). Also the conversion of original model from Protein Data Bank into electron density could be implemented in order to compare it to the reconstructed object.

6. Acknowledgements

I would like to acknowledge Max Rose and Dmitry Dzhigaev for their intense support, help and patience during all summer program, Ivan Vartanians for supervising me. I would also like to thank Max Rose, Dmitry Dzhigaev, Anatoly Shabalin, Oleg Gorobtsov, Ivan Zaluzhnyy, Sergey Lazarev and Ivan Vartanians for fruitful discussions and answering my questions.

I also thank Edgar Weckert for providing me with MOLTRANS program and consulting on it, Dmitry Dzhigaev for providing with phase retrieval algorithms' code PHASOR. Additionally, I would like to thank Olaf Behnke and all Summer Student Programme 2016 organising team for such unforgettable time in Hamburg.

References

- [1] Massimo Altarelli, R Brinkmann, M Chergui, W Decking, B Dobson, S Düsterer, G Grübel, W Graeff, H Graafsma, J Hajdu, et al. The european x-ray free-electron laser. *Technical Design Report, DESY*, 97:1–26, 2006.
- [2] Evgeny Saldin, EV Schneidmiller, and Mikhail V Yurkov. *The physics of free electron lasers*. Springer Science & Business Media, 2013.
- [3] Richard Neutze, Remco Wouts, David van der Spoel, Edgar Weckert, and Janos Hajdu. Potential for biomolecular imaging with femtosecond x-ray pulses. *Nature*, 406(6797):752–757, 2000.
- [4] Henry N Chapman, Anton Barty, Michael J Bogan, Sébastien Boutet, Matthias Frank, Stefan P Hau-Riege, Stefano Marchesini, Bruce W Woods, Saša Bajt, W Henry Benner, et al. Femtosecond diffractive imaging with a soft-x-ray free-electron laser. *Nature Physics*, 2(12):839–843, 2006.
- [5] Ne-Te Duane Loh and Veit Elser. Reconstruction algorithm for single-particle diffraction imaging experiments. *Physical Review E*, 80(2):026705, 2009.
- [6] RCSB PDB - 1UF2. the atomic structure of rice dwarf virus (rdv). <http://www.rcsb.org/pdb/explore.do?structureId=1uf2>. Accessed: 2016-09-02.
- [7] VD Sivuhin. *General physics course. Optics*. Moscow: Nauka, 1979.
- [8] Euler angles. wikipedia, the free encyclopedia. https://en.wikipedia.org/wiki/Euler_angles. Accessed: 2016-09-03.
- [9] Euler Angles – from wolfram mathworld. <http://mathworld.wolfram.com/EulerAngles.html>. Accessed: 2016-09-03.
- [10] James R Fienup. Phase retrieval algorithms: a comparison. *Applied optics*, 21(15):2758–2769, 1982.
- [11] Harry Nyquist. Certain topics in telegraph transmission theory. 1928.
- [12] Claude Elwood Shannon. Communication in the presence of noise. *Proceedings of the IRE*, 37(1):10–21, 1949.
- [13] Joseph W Goodman. *Introduction to Fourier optics*. Roberts and Company Publishers, 2005.
- [14] Ron Bracewell. *The Fourier Transform and its Applications*, volume 5. 1965.

Appendix A. Fourier transform

A lot of physical phenomena have the property of *linearity*. It means that the overall response of the system is equal to the superposition of different responses that each element of this system would produce individually. Amongst these phenomena there are: electrical networks composed of main electrical elements (resistors, capacitors, inductors), propagation of light through most media, description of the state of the particle as a wave function in quantum mechanics, etc.

One of the main mathematical tools for analysing linear phenomena is called *Fourier transform*. The *Fourier transform* of a function (in general, complex-valued) g in one dimensional case is represented as $\mathcal{F}(g)$ (or $\hat{g}(\omega)$) and defined by

$$\mathcal{F}(g) = \hat{g}(\omega) = \frac{1}{\sqrt{2\pi}} \int_{-\infty}^{\infty} g(x) \exp(-i\omega x) dx \quad (15)$$

where $\omega = 2\pi f$ is the angular frequency.

In two dimensional case:

$$\mathcal{F}(g) = \hat{g}(\omega_x, \omega_y) = \frac{1}{2\pi} \iint_{-\infty}^{\infty} g(x, y) \exp(-i(\omega_x x + \omega_y y)) dx dy \quad (16)$$

In three dimensional case:

$$\mathcal{F}(g) = \hat{g}(\omega_x, \omega_y, \omega_z) = \frac{1}{(2\pi)^{3/2}} \iiint_{-\infty}^{\infty} g(x, y, z) \exp(-i(\omega_x x + \omega_y y + \omega_z z)) dx dy dz \quad (17)$$

or, by extension,

$$\mathcal{F}(g) = \hat{g}(\vec{\omega}) = \frac{1}{(2\pi)^{n/2}} \int_{-\infty}^{\infty} g(\vec{r}) \exp(-i(\vec{\omega} \cdot \vec{r})) d\vec{r}^n \quad (18)$$

where n is the number of dimensions.

The *inverse Fourier transform* can be represented as

$$\mathcal{F}^{-1}(\hat{g}) = g(\vec{r}) = \frac{1}{(2\pi)^{n/2}} \int_{-\infty}^{\infty} \hat{g}(\vec{\omega}) \exp(i(\vec{\omega} \cdot \vec{r})) d\vec{\omega}^n \quad (19)$$

In general words one can say that the *Fourier transform* decomposes the function into simple harmonic functions that make it up. These harmonic functions look like

$$A(\vec{\omega}) \exp(i(\vec{\omega} \cdot \vec{r})) \quad (20)$$

where $A(\vec{\omega})$ is the amplitude and $\vec{\omega} \cdot \vec{r}$ is the phase offset from the basic sinusoid of the same frequency.

As for the light propagation, every light wave is regarded as a superposition of plane waves of the form 20

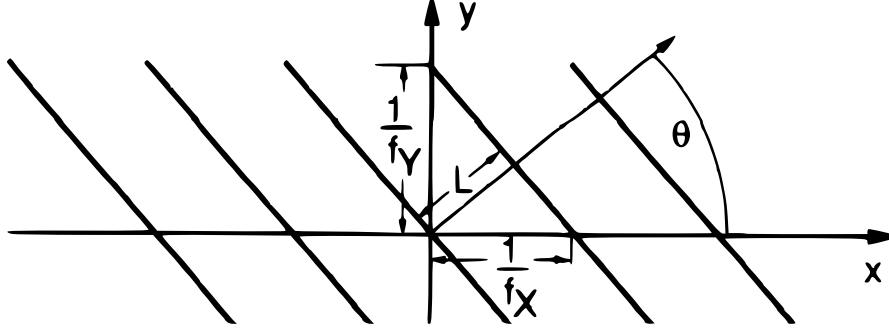


Figure 11: A plane wave. Lines of zero phase for the function $\exp(2\pi i(f_x x + f_y y))$ are shown. [13]

The *discrete Fourier transform* for a 1D array of size N is defined as

$$\mathcal{F}(g) = \hat{g}_k = \frac{1}{\sqrt{N}} \sum_{m=0}^{N-1} g_m \exp\left(-2\pi i k \frac{m}{N}\right). \quad (21)$$

The *inverse discrete Fourier transform* for a 1D array of size N is defined as

$$\mathcal{F}^{-1}(\hat{g}) = g_k = \frac{1}{\sqrt{N}} \sum_{m=0}^{N-1} \hat{g}_m \exp\left(2\pi i k \frac{m}{N}\right). \quad (22)$$

For more-dimensional arrays it is defined on the analogy with Fourier transform for continuous functions.

For more detailed information see Goodman [13] and Bracewell [14].